



HAL
open science

A combined $2\omega/3\omega$ method for the measurement of the in-plane thermal conductivity of thin films in multilayer stacks: Application to a silicon-on-insulator wafer

F. Mazzelli, J. Paterson, F. Leroy, O. Bourgeois

► To cite this version:

F. Mazzelli, J. Paterson, F. Leroy, O. Bourgeois. A combined $2\omega/3\omega$ method for the measurement of the in-plane thermal conductivity of thin films in multilayer stacks: Application to a silicon-on-insulator wafer. *Journal of Applied Physics*, 2025, 137 (1), pp.015106. 10.1063/5.0227482 . hal-04877691

HAL Id: hal-04877691

<https://hal.science/hal-04877691v1>

Submitted on 9 Jan 2025

HAL is a multi-disciplinary open access archive for the deposit and dissemination of scientific research documents, whether they are published or not. The documents may come from teaching and research institutions in France or abroad, or from public or private research centers.





L'archive ouverte pluridisciplinaire **HAL**, est destinée au dépôt et à la diffusion de documents scientifiques de niveau recherche, publiés ou non, émanant des établissements d'enseignement et de recherche français ou étrangers, des laboratoires publics ou privés.



Distributed under a Creative Commons Attribution 4.0 International License

RESEARCH ARTICLE | JANUARY 03 2025

A combined $2\omega/3\omega$ method for the measurement of the in-plane thermal conductivity of thin films in multilayer stacks: Application to a silicon-on-insulator wafer

F. Mazzelli; J. Paterson ; F. Leroy ; O. Bourgeois  



J. Appl. Phys. 137, 015106 (2025)

<https://doi.org/10.1063/5.0227482>



Articles You May Be Interested In

Thermal conductivity and thermal boundary resistance of amorphous Al_2O_3 thin films on germanium and sapphire

J. Appl. Phys. (June 2020)

Specific heat measurement of thin suspended SiN membrane from 8 K to 300 K using the 3ω -Völklein method

Rev. Sci. Instrum. (September 2013)

Simultaneous measurement of in-plane and through-plane thermal conductivity using beam-offset frequency domain thermoreflectance

Rev. Sci. Instrum. (January 2017)



Journal of Applied Physics

Special Topics Open for Submissions

[Learn More](#)

A combined $2\omega/3\omega$ method for the measurement of the in-plane thermal conductivity of thin films in multilayer stacks: Application to a silicon-on-insulator wafer

Cite as: J. Appl. Phys. 137, 015106 (2025); doi: 10.1063/5.0227482

Submitted: 9 July 2024 · Accepted: 12 December 2024 ·

Published Online: 3 January 2025



View Online



Export Citation



CrossMark

F. Mazzelli,^{1,2} J. Paterson,^{1,2,a)}  F. Leroy,³  and O. Bourgeois^{1,2,b)} 

AFFILIATIONS

¹Institut Néel, CNRS, 25 avenue des Martyrs, Grenoble 38042, France

²Université Grenoble Alpes, Institut Néel, Grenoble 38042, France

³Centre Interdisciplinaire de Nanoscience de Marseille, Aix-Marseille Université, Marseille 13288, France

^{a)}Present address: Department of Physics, University of California Berkeley, Berkeley, CA 94720, USA

^{b)}Author to whom correspondence should be addressed: olivier.bourgeois@neel.cnrs.fr

ABSTRACT

This study focuses on establishing and validating a method to accurately measure the in-plane thermal conductivity of very conductive thin films, such as single-crystal metals or semiconductors, 2D and nanostructured materials. By integrating both 2ω and 3ω measurements, the method is rendered insensitive to the superficial thermal boundary resistance of the insulating overlayer, enabling precise estimation of the in-plane thermal properties of conductive films grown on top of substrates or multilayer stacks. The proposed technique is applied to analyze the thermal conductivity of a silicon-on-insulator stack with a top layer consisting of a 340 nm thick film of monocrystalline silicon. Measurements are conducted within a temperature range spanning from 250 to 325 K. The results confirm the method's capability to correctly assess the thermal conductivity decrease of the silicon film compared to bulk value, demonstrating its reliability for the thermal characterization of conductive thin films.

© 2025 Author(s). All article content, except where otherwise noted, is licensed under a Creative Commons Attribution (CC BY) license (<https://creativecommons.org/licenses/by/4.0/>). <https://doi.org/10.1063/5.0227482>

I. INTRODUCTION

Semiconductor thin films have become ubiquitous across different technological domains, including integrated circuits and microelectronics, thermoelectric devices, actuators, and sensors.^{1,2} In most of these applications, thermal transport remains a critical issue, impacting the long-term performance and reliability of devices.¹

Thermal issues are especially critical when thin films are fabricated on top of insulating oxide layers, such as in Silicon-On-Insulator (SOI) or Germanium-On-Insulator (GOI) stacks, where heat dissipation is significantly hindered by the low thermal conductivity of the buried oxide (BOX) and by the reduced thermal conductivity in the thin semiconducting layer.³ Consequently, developing new experimental methods to determine

the in-plane thermal properties of the conductive layer is essential for both engineering design purposes and for providing reliable data to validate numerical and phenomenological models.

Yet, achieving accurate measurements of the thermal conductivity of highly conductive thin films presents significant challenges, particularly at the nanoscale. Traditional electro-thermal methods like the 3ω technique face limitations in sensitivity since the temperature difference measured in 3ω is mostly affected by the more resistive layers. Even when the film to be measured is poorly conductive, signals can be overshadowed by the thermal resistance of the passivating layer or any other thermal boundary resistance (TBR) within the sample. These resistances act as a barrier to heat flow, affecting the measured temperature difference and resolution of the overall thermal measurement.

06 January 2025 08:00:23

Recognizing the limitation of regular 3ω methods, Ramu and Bowers⁴ proposed the 2ω method as a simpler alternative to measure thermal conductivities of thin films. The technique offers enhanced sensitivity to the in-plane thermal conductivities and minimizes the influence of the thermal contact resistance between the sample and the thermometer. This last point is especially important since, as mentioned above, the thermal resistance of passivating overlayers is what drastically increases uncertainty of 3ω measurements.

The 2ω method is ideally suited to measure the thermal properties of thin films grown atop insulating materials, which thermally decouple the film from the substrate, like in SOI or GOI stacks. In these cases, most of the heat is conducted by the layers above the oxide, rendering the 2ω method extremely sensitive to the in-plane thermal conductivity of the film to be measured. However, multilayer stacks pose challenges during data analysis due to the complication of fitting multiple unknown thermal properties.

One possible way around these issues may come from using freestanding membranes.^{5–9} This approach allows for effectively decoupling the thin film from the substrate without the need for insulating oxide layers. However, other than being more technologically complex, experiments on suspended samples may potentially lead to differing results compared to tests performed on non-suspended samples. Indeed, experimental evidence⁸ has shown that thermal conductivities of SOI thin films are systematically higher than those of freestanding membranes. Moreover, for very thin membranes (<10 nm thickness), the suspended architecture leads to modifications in the phonon dispersion relations, giving rise to additional flexural modes that are absent in bulk materials.⁹

Consequently, the development of experimental techniques to study the thermal properties of low-dimensional materials remains an open problem and new methods should be sought that potentially avoid difficulties of suspended samples and, at the same time, reduce problems related to the presence of surface passivating layers.

In this work, we address these limitations by employing a careful combination of independent 2ω and 3ω measurements. This approach allows extracting all thermal parameters within a multilayer stack with minimal uncertainty. We have applied the method on an SOI sample with 340 nm thick monocrystalline Si overlayer grown atop a $1\mu\text{m}$ thick layer of silicon dioxide. The results confirmed the substantial insensitivity of the measurements to the superficial and intermediate TBRs and enabled an accurate estimation of the crystalline Si film thermal conductivity decrease with respect to the bulk.

II. PROPOSED APPROACH: COMBINING 2ω AND 3ω METHODS FOR REDUCED UNCERTAINTY

The 2ω method⁴ is an experimental alternative to the 3ω method that has been used to study thermally anisotropic bulk materials^{4,10} or to probe the phonon mean-free-path spectrum of semiconducting films.¹¹ Similar to the 3ω method, the 2ω approach involves a metal line deposited on the sample surface that generates temperature oscillations at a frequency of 2ω . The primary distinction from the standard 3ω method lies in the use of two parallel

resistances instead of a single metal line, with one serving as a heater and the other functioning as a temperature transducer, as illustrated schematically in Fig. 1. Furthermore, unlike the 3ω method—which detects temperature oscillations by measuring the third harmonic of the voltage signal—the 2ω method determines temperature oscillations by directly measuring the second harmonic of the voltage acquired by the second transducer (additional details on the 2ω method are provided in Secs. III–V).

The major advantages of the 2ω method are a higher sensitivity to the in-plane thermal conductivity and an insensitivity to the boundary thermal resistance at the interface between the thermometer and the sample. Physically, this is because the temperature gradient is approximately perpendicular to the interface beneath the heater and approximately parallel to the interface beneath the thermometer.⁴ Consequently, the thermometer is less influenced by thermal properties that affect the temperature change in a direction perpendicular to the surface (e.g., changes in the superficial TBR), while it is most sensitive to those that impact the heat transport parallel to it (e.g., changes in the thermal conductivity due to thinning of the film thickness). The resulting advantages of high sensitivity to the in-plane thermal conductivity and insensitivity to superficial TBR make up for an ideal technique to study the thermal conductivity of highly conductive thin films. This includes films whose thickness is such that thermal conductivity is limited by boundary scattering phenomena, like the thin films considered in this study (challenges may arise when the thickness of the film is reduced to the extent that the thermal conductance of the layer becomes too low. In such cases, insufficient heat flow through the film can impede accurate detection and limit the effectiveness of the technique for measuring ultrathin films and 2D materials).

A clear disadvantage of the 2ω method compared to the classical 3ω is the necessity of two separate transducers, leading to the requirement for additional equipment to conduct measurements (such as additional current sources, wiring, and access ports to test sections). Moreover, the need for two metal transducers potentially introduces further uncertainties related to the width of the second transducers and the heater/thermometer inter-distance. However, these additional parameters also offer valuable degrees of freedom in designing the heater/thermometer pair: by adjusting both the

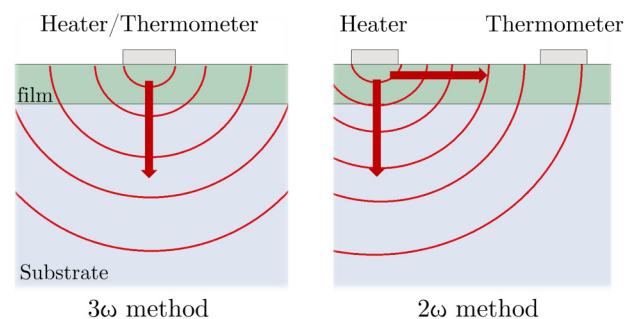


FIG. 1. Comparison between 3ω and 2ω methods. The 3ω method is mostly sensitive to the cross-plane thermal conductivity, whereas the 2ω method has higher sensitivity to the in-plane thermal conductivity.

transducers distance and width, the sensitivity of the setup can be maximized to target the measurement of specific layers.

Building upon the work of previous authors,¹² we used this dual degree of freedom to design two pairs of heating/sensing lines that are selectively sensitive to different layers of a SOI stack, as we will elaborate shortly. The first of these two designs allows, alone, to extract the substrate's thermal conductivity with precision. The second pair is designed to have maximal sensitivity to the thin film in-plane thermal conductivity. However, despite this enhanced sensitivity, the second design alone is not sufficient for the extraction of the Si overlayer properties, which requires additional information regarding the thermal conductivity of the BOX (but, as we will show, no information is needed about the superficial TBR).

To access this information, the same transducers designed for the 2ω tests can be used to perform classical 3ω measurements of the intermediate insulating layer. This is the approach followed in Ref.¹², and it has the advantage of obtaining all the required data using the same two couples of sensors. However, during our campaign, we noted that this approach often led to considerable uncertainty.

The reason for this has partly to do with the propagation of uncertainty. Due to its position as a superficial layer, the determination of the Si overlayer thermal conductivity depends on the measured properties of other layers composing the SOI. Consequently, even a modest uncertainty on the fit of beneath layers produces, in cascade a high uncertainty in the estimation of the Si film thermal properties. Moreover, the additional 3ω measurements needed to extrapolate the BOX thermal conductivity (as in the approach of Ref. 12) do possess some dependence on the superficial and intermediate TBRs, which brings back the problem of their assessment. The combined effect of propagated uncertainty and sensitivity to TBR can lead to a final uncertainty for the thin film thermal conductivity that is of the same order as its reduction due to low dimensional effects.

To avoid this issue, in our work, we opted for separate measurements of the BOX layer, following a well-established procedure of our lab (more details on this are provided in later sections and in the [supplementary material](#), Secs. III–IV). At the expense of some additional tests, this approach allowed us to completely disregard the effect of the sample's TBRs and to estimate the intrinsic (thickness-independent), in-plane thermal conductivity of the crystalline Si overlayer with a low degree of uncertainty.

The proposed approach was applied on a SOI stack, whose layer composition is depicted in Fig. 2. From bottom to top, the sample is composed of a $525\ \mu\text{m}$ -thick substrate of monocrystalline Si, followed by a $1\ \mu\text{m}$ -thick layer of SiO_2 electrically insulating oxide. The monocrystalline silicon overlayer is $340\ \text{nm}$ thick, on top of which we deposit a $60\ \text{nm}$ thick film of alumina (Al_2O_3) to prevent current in the transducers from leaking into the sample. The gray box on top of the sample represents the sensing/heating line, a $295\ \text{nm}$ thick layer of Pt below which is deposited a $5\ \text{nm}$ thick layer of Ti, whose purpose is to promote adhesion between the metal and the alumina layer. The complete specifications of the SOI stack are provided in Sec. 1 in the [supplementary material](#).

Finally, for later use, we define here the superficial and intermediate TBRs depicted in Fig. 2 as the following thermal

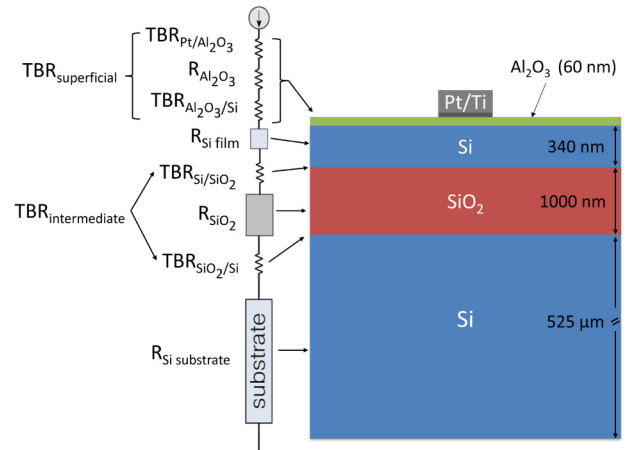


FIG. 2. SOI layer composition, the green film is the alumina capping layer needed to insulate the transducer from the conductive Si layer. On the left side is represented a simplified equivalent thermal model of the stack.

resistances:

$$\begin{aligned} TBR_{\text{superficial}} &= TBR_{\text{Pt/Al}_2\text{O}_3} + \frac{t_{\text{Al}_2\text{O}_3}}{k_{\text{Al}_2\text{O}_3}} + TBR_{\text{Al}_2\text{O}_3/\text{Si}}, \\ TBR_{\text{intermediate}} &= TBR_{\text{Si/SiO}_2} + TBR_{\text{SiO}_2/\text{Si}}. \end{aligned} \quad (1)$$

III. MATERIALS AND METHOD

A. Modeling the material thermal response

Extracting thermal conductivities using the 3ω and 2ω methods requires comparing our experimental data with results from a thermal model of the SOI stack. In our work, we make use of the so-called “Thermal Quadrupole” method, which was initially proposed by Carslaw and Jaeger¹³ and later refined by different authors (see, for instance, Ref. 14).

The idea behind this approach is to consider a series of infinitely wide slabs of varied materials, whose properties are considered uniform within each slab. Figure 3 illustrates a schematic of the model. The 2D heat flux across each layer is then expressed by considering as boundary conditions the incoming flux and the temperature of each preceding layer. The process is recursively repeated and formally closed when the last layer is reached, where either isothermal or adiabatic boundary conditions are applied.

The result of this procedure is a complex matrix product that returns the average temperature oscillation sensed by the transducer as a function of the thermal properties of each material slab and the boundary conditions (BCs). In the case of 2ω geometry, the temperature difference at the sample surface, for different BC at the bottom surface, is given by

$$\langle \Delta T \rangle_{2\omega\text{-isoth}} = \frac{P_1}{2b_1 b_2 \pi} \int_{-\infty}^{\infty} \frac{\sin(\lambda b_1) \sin(\lambda b_2)}{\lambda^2} \frac{B}{D} e^{i\lambda d_{ht}} d\lambda, \quad (2a)$$

$$\langle \Delta T \rangle_{2\omega\text{-adiab}} = \frac{P_1}{2b_1 b_2 \pi} \int_{-\infty}^{\infty} \frac{\sin(\lambda b_1) \sin(\lambda b_2)}{\lambda^2} \frac{A}{C} e^{i\lambda d_{ht}} d\lambda, \quad (2b)$$

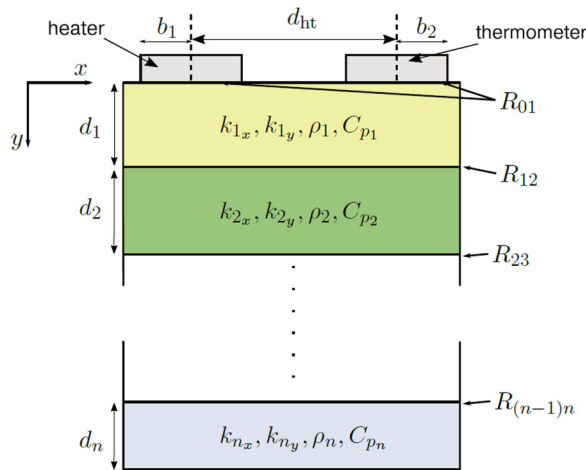


FIG. 3. General scheme for the resolution of the heat equation inside a multilayered material.

where P_j is the power per unit length (W m^{-1}) dissipated by the heater, d_{ht} is the distance between the thermometer and the heater midlines, b_1 and b_2 are the heater and thermometer half-widths, and λ is the Fourier transform integration variable.

The reason for the angle brackets around the temperature oscillation $\langle \Delta T \rangle$ is that the formulation given here returns a spatially averaged temperature amplitude along the thermometer width. This is, indeed, the temperature of interest, which must be compared to the measured temperature oscillation.

The coefficients A , B , C and D represent the result of the matrix calculations and are given by

$$\begin{aligned} \begin{pmatrix} A & B \\ C & D \end{pmatrix} &= \prod_{j=1}^n \begin{pmatrix} 1 & R_{(j-1)j} \\ 0 & 1 \end{pmatrix} \\ &= \begin{pmatrix} \cosh(\gamma_j d_j) & \frac{1}{k_{jy} \gamma_j} \sinh(\gamma_j d_j) \\ k_{jy} \gamma_j \sinh(\gamma_j d_j) & \cosh(\gamma_j d_j) \end{pmatrix}, \quad (3) \\ \gamma_j &= \sqrt{\frac{k_{jx}}{k_{jy}} \lambda^2 + i \omega_T \frac{(\rho c_p)_j}{k_{jy}}}, \end{aligned}$$

where $R_{(j-1)j}$ is the TBR between the $(j-1)$ th and j th layer, d_j is the thickness of the j th slab, k_{jy} and k_{jx} are the cross-plane and in-plane thermal conductivities, ρc_p is the product of the density and the specific heat of the layer, and ω_T is the thermal angular frequency, defined as twice the electrical angular frequency.

Various comments are in need to properly frame the use of this mathematical model.

- Equation (2) is both valid for 2ω and 3ω geometries. When the heater/transducer distance is set to zero and their width is equal, the solution of the model represents the temperature oscillation as sensed by a classical 3ω measurements. It is equivalent to the

solution given by Borca-Tasciuc *et al.*,¹⁵ but with thermal boundary resistances included.

- The model is 2D as it assumes an infinitely long metal line. For this reason, the fabricated metal lines used in our experiments have high aspect ratios (i.e., length much greater than the width). For the same reason, the voltage difference is always measured at the inner leads of a four-wire sensor configuration. The inner leads are placed far from the outer pads to reduce thermal edge effects due to heat conduction along the wires and pads¹⁶ (see Sec. 4 in the [supplementary material](#) for details on the transducers designs).
- The present model can be extended to include the third dimension as shown in Sec. 2 in the [supplementary material](#). The model is then able to account for the finiteness of the transducers' length. In our study, we mostly used the 2D version of the model for faster calculations. Nevertheless, the 3D model was used to assess the appropriateness of the 2D assumption and to analyze the impact of edge effects on the measured temperature oscillation.
- Solving Eq. (2) implies calculating complex integral transforms. Some analytical solutions exist for simple cases like the semi-infinite substrate that involve the use of Bessel functions. However, for the general case, numerical integration is necessary. Section 2 of the [supplementary material](#) provides some hints to facilitate the numerical integration of Eq. (2).

Finally, it is important to stress the crucial role of this thermal model, which in our work is used both as a fitting tool, to analyze the experimental data and extrapolate the values of the material conductivities, as well as a design tool, to perform the sensitivity analysis and choosing the best design configuration for our experiment, as explained in Sec. III B.

B. Sensitivity analysis and transducers design

The proposed 2ω approach involves a preliminary design phase for the heater/transducer pairs. The design process aims to maximize the sensitivity of a given geometry to a specific target layer in the stack. This is achieved by varying the transducer widths and the distance between the thermometer and heater.

In our analysis, we use a scaled sensitivity, defined as follows:

$$S'_x = x \cdot \frac{\partial \Delta T}{\partial x},$$

where x represents a generic quantity for which the sensitivity is calculated (e.g., the thermometer width).

This definition accounts for the impact of temperature oscillation damping with increasing distance from the heater and is, therefore, more suited to sensitivity analyses involving the 2ω method. Section 3 in the [supplementary material](#) provides more details on this definition.

To calculate the sensitivities to the parameters of interest, the thermal model presented in Sec. III A is implemented in MATLAB R2022b.¹⁷ The program can work in 3ω and 2ω configurations, in three or two dimensions, and with isothermal or adiabatic BC. It takes as input the thermal properties of a multilayer stack and automatically calculates the matrix of coefficient of Eq. (3) for any

desired number of layers. To find the optimal layouts of the heater/transducer couples, the code computes the sensitivities to all thermophysical properties as a function of the distance heater/thermometer and for different widths of the transducers.

Table I gives the thermal properties used for each SOI layer in the preliminary design process. The data for thermal conductivity and heat capacities represent average values from the literature.^{18,19} By contrast, the thermal boundary resistances are generally not known since they depend on the microscale morphological details of the interface, which are influenced by the specific manufacturing process. To estimate the heat resistance of the 60 nm alumina layer, we used values obtained during previous tests of our group.²⁰ For the intermediate TBRs, we used an expected value of $1 \times 10^{-8} \text{ m}^2 \text{ K}^{-1} \text{ W}^{-1}$, but higher values (up to $3 \times 10^{-8} \text{ m}^2 \text{ K}^{-1} \text{ W}^{-1}$) were also tested to confirm the insensitivity to this parameter.

It is further worth noticing that, in our approach, the thin layer of alumina is not considered as a separate material, but its thermal resistance is included within the superficial TBR [see Fig. 2 and Eq. (1)]. There are a few good reasons for doing so. The first is that the layer of alumina is so thin that its heat capacity is negligible. For massless films, it is possible to simplify the mathematical approach by considering the layer as a pure heat resistance put in series with respect to the heat flow direction, allowing for a simplified modeling approach. The second reason is that, by reducing the number of variables at play, the fitting process can be greatly simplified. Finally, the thermal response of 2ω measures is insensitive to practically any value of the superficial TBR, thus making its knowledge unnecessary in our approach.

Figure 4 presents the sensitivity trends calculated for a large thermometer ($40 \mu\text{m}$ wide) in 2ω configurations at 180 Hz as a function of the heater/thermometer distance. The sensitivity curves account for both the in-plane and cross-plane thermal conductivities of the Si overlayers since both parameters are of interest for the thermal characterization of the thin film. By contrast, heat capacities are excluded from the sensitivity analysis since we found that they play a negligible role in determining the temperature oscillation sensed by the thermometer for any of the tested configurations.

Looking at Fig. 4, a thermometer placed at around $60 \mu\text{m}$ from the heater is only sensitive to the thermal conductivity of the substrate. Therefore, a configuration consisting of a Thermometer at Large Distance from the heater (TLD from now on) can be profitably used to infer the thermal properties of the substrate.

Similarly, Fig. 5 illustrates the sensitivities calculated for a narrow transducer ($8 \mu\text{m}$ wide) in 2ω configuration and for

TABLE I. Thermal properties used during the design phase. The TBR of the first layer includes the 60 nm alumina layer and is estimated using measured data from Ref. 20.

Layer	Thermal conductivity ($\text{W m}^{-1} \text{K}^{-1}$)	Volumetric heat capacity ($\text{MJ m}^{-3} \text{K}^{-1}$)	TBR ($\text{m}^2 \text{K}^{-1} \text{W}^{-1}$)
1st	140	1.62	6.5×10^{-8}
2nd	1.4	1.64	1×10^{-8}
3rd	140	1.62	1×10^{-8}

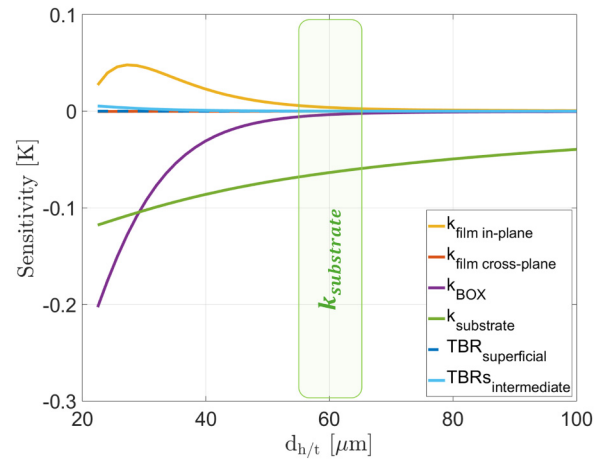


FIG. 4. Sensitivity trends calculated for a $40 \mu\text{m}$ wide thermometer in 2ω configuration at 180 Hz and for different heater/thermometer distances: the thermometer at large distance from the heater is selectively sensitive to the thermal conductivity of the substrate alone.

different heater/thermometer distances. At around $15 \mu\text{m}$ from the heater, the sensitivity to the in-plane thermal conductivity of the upper film is maximized. Consequently, a configuration of a Thermometer at Short Distance from the heater (TSD from now on) is retained to study the effect of the in-plane thermal conductivity of the first layer.

In total, two heater/thermometer pairs were selected for our study. One pair includes a wide thermometer placed at a large distance from the heater, while the other pair consists of two narrow

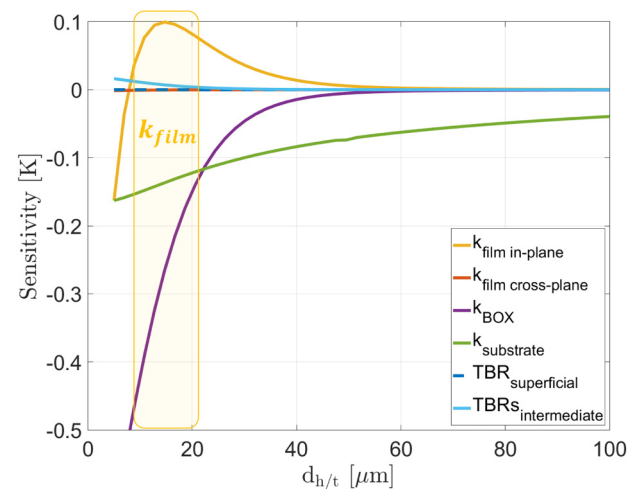


FIG. 5. Sensitivity trends calculated for a $8 \mu\text{m}$ wide thermometer in 2ω configuration at 180 Hz and for different heater/thermometer distances: a thermometer at a short distance maximizes the sensitivity to the in-plane thermal conductivity of the thin film.

06 January 2025 08:00:23

transducers positioned close to each other; these transducers are identical and can function as either a heater or a thermometer. Additionally, our procedure requires a separate design for the 3ω measurements of the BOX, as explained in Sec. II. Section 4 of the [supplementary material](#) illustrates the final geometries of all transducers used in our study along with details on the nanofabrication process employed to deposit the transducers onto the samples.

C. Data fitting procedure

Assuming that the silicon substrate and the insulating amorphous layer have no thermal anisotropy, six independent parameters must be input into the model for fitting the experimental data. Of these, the $k_{film, cross-plane}$ and the superficial and intermediate TBRs [this last considered as one parameter including both intermediate TBRs, as for Eq. (1)] do not affect the fitting of experimental data and their value can be simply chosen with some reasonable estimates or from literature data. This leaves three independent parameters to be fitted by as many independent measurements. These parameters are the thermal conductivities of the BOX and the substrate, as well as the in-plane thermal conductivity of the Si overlayer.

The measurement and fitting procedure of the three required thermal properties is conducted as follows:

1. First, 2ω experiments with both TLD and TSD configurations are performed on the SOI stack. However, only the data of the TLD transducer are fitted in this phase to obtain the substrate thermal conductivity. This is possible since this configuration is insensitive to any parameter except the Si substrate thermal conductivity.
2. The 3ω experiments are conducted on different SOI samples in which the overlayer is removed and the BOX is thinned in four different thicknesses. Using the previously calculated substrate's conductivity, these experiments are fitted to obtain silica thermal conductivity. In addition, an estimate of the TBRs between silica and silicon can be obtained as well.
3. With the knowledge of the substrate and BOX thermal conductivities, the 2ω experiments of the TSD can be fitted to obtain the in-plane thermal conductivity of the Si film.

Data fitting may then be iterated by entering the new calculated values for the various layers and updating the results for each step. However, this process generally produces negligible changes to final values since the 2ω experiments for the substrate and the BOX directly give the right results at the first iteration. [Table II](#) summarizes the fitting procedure while Sec. 5 in the [supplementary material](#) gives additional explanations for step 2.

Finally, it is worth emphasizing once more the absence of the surface TBR among the parameters to be fitted. This characteristic is crucial as it reduces uncertainty in the fitting process and lessens the requirement for multiple independent measurements. By contrast, the method's lack of sensitivity to $k_{film, cross-plane}$ may be a limitation in certain applications, as it hinders its use for direct assessment of thermal anisotropy in highly conductive thin films grown on substrates. The combination with the 3ω method may also not lead to accurate results in this respect since the measurement of the film's cross-plane thermal conductivity via the 3ω

TABLE II. Summary of the measurements used to extract the different thermal properties. Three out of the six thermal parameters can be known, leaving out the film cross-plane thermal conductivity and the TBRs, whose knowledge is not needed in the proposed approach.

Measurement type	Sensor design	Extracted parameter	Fitting step	Left-out parameters
2ω	TLD	$k_{substrate}$	1s	$k_{film, cross-plane}$
2ω	TSD	$k_{film, in-plane}$	3rd	$TBR_{superficial}$
3ω	Single sensor	k_{BOX}	2nd	$TBR_{intermediate}$

method could be hindered by the low cross-plane thermal resistance and the influence of the superficial TBR. In the authors' view, the feasibility of using this technique to directly measure anisotropic "film on substrate" may be very material dependent, with possible application to films that allow achieving enough sensitivity on both the cross-plane and in-plane directions (for the others, the only feasible way may involve the use of suspended samples or advanced optical techniques). Consequently, this paper focuses on measuring the "in-plane" thermal conductivity of thin films rather than addressing the broader challenge of determining their thermal anisotropy (nevertheless, the 2ω method can still be used to measure thermal anisotropy of "bulk" materials, as demonstrated by the work of previous authors^{4,10}).

D. Experimental setup for 2ω and 3ω measurements

The experimental setup for the 3ω method is illustrated in [Fig. 6](#). In this setup, a programmable resistor is put in series with the thermometer, considerably reducing the high background $V_{1\omega}$ signal via a differential bridge. The subtracted signal is then amplified by a series of low-noise amplifiers that give a total gain of 6.25. This allows accurate reading of $V_{3\omega}$ by the lock-in amplifier, which exploits the maximum of its dynamic reserve to capture the signal while extracting it out from undesired noise sources.

The temperature oscillation experienced by the metal transducer is related to the $V_{3\omega}$ signal sensed by the lock-in amplifier

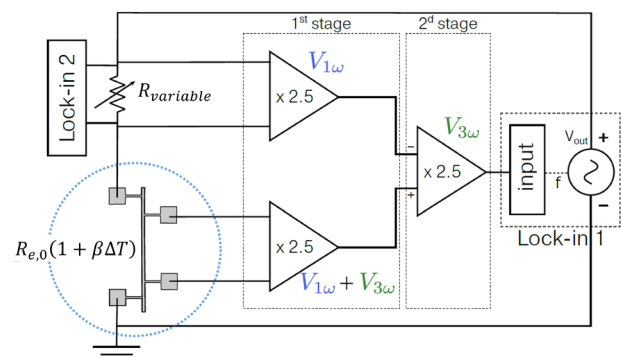


FIG. 6. Scheme of the 3ω method setup with compensation of the $V_{1\omega}$ component using a differential bridge.

06 January 2025 08:00:23

according to the following relation:²¹

$$\Delta T_{2\omega} = \frac{2V_{3\omega}}{R_{e,0}\beta(T)I_{1\omega}}, \quad (4)$$

where $I_{1\omega} = I_{ac}\cos(\omega t)$ is the alternating current at an angular frequency ω circulating across the circuit, $R_{e,0}$ is the electrical resistance of the thermometer at a reference temperature T_0 and for a zero current input, and $\beta(T)$ is known as the temperature coefficient of resistance (TCR) of the thermometer. These last two parameters are defined by the linear approximation that express the dependence of the transducer's electrical resistance to its temperature,

$$R_e(T) = R_{e,0} \left(1 + \frac{1}{R_{e,0}} \left. \frac{dR}{dT} \right|_{T_0=0} \cdot (T - T_0) \right) = R_{e,0} (1 + \beta(T) \cdot \Delta T). \quad (5)$$

Equation (4) establishes a relation between the third harmonics of the voltage oscillation at the thermometer leads and the temperature oscillation at the material surface. It is by comparing this temperature oscillation with the values predicted by the thermal model [Eq. (2)] that we infer the thermal properties of the sample.

Figure 7 depicts the scheme of the 2ω setup. The main difference with the standard 3ω method is that instead of a single metal line used to heat and sense the sample, two parallel metal lines are used, one acting as a heater and the other as a temperature sensor.

The experiment proceeds as follows: an AC current at electrical angular frequency ω passes through a metallic line of electrical resistance $R_{e,heat}(T)$ which serves as a heater. The resulting Joule heating leads to a temperature oscillation at 2ω that propagates through the sample being tested. This temperature oscillation is measured using a nearby transducer of resistance $R_{e,th}(T)$, which is driven by a DC current. We use two lock-in amplifiers, one for measuring the heating power and a second to sense the voltage oscillation along the thermometer.

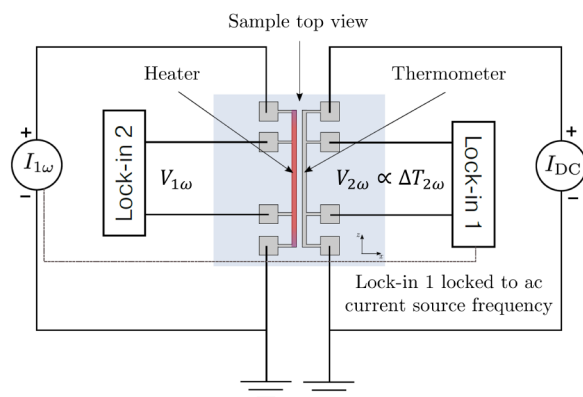


FIG. 7. Scheme of the 2ω method setup.

The voltage measured across the thermometer is then comprised of a DC component on top of which is superimposed an AC voltage difference due to the oscillating temperature field,

$$\begin{aligned} V &= R_{e,Th}I_{DC} = R_{e,0}(1 + \beta(T)\Delta T_{DC} + \beta(T)\Delta T_{2\omega})I_{DC} \\ &= R_{e,0}(1 + \beta(T)\Delta T_{DC})I_{DC} + R_{e,0}\beta(T)\Delta T_{2\omega}I_{DC} \\ &= V_{DC} + V_{2\omega}. \end{aligned} \quad (6)$$

From this, it immediately follows:

$$\Delta T_{2\omega} = \frac{V_{2\omega}}{R_{e,0}\beta(T)I_{DC}}. \quad (7)$$

Therefore, measuring voltage oscillations at 2ω allows determination of temperature oscillations at the sample surface. Analogous to the 3ω method, the comparison of the measured temperature oscillation with thermal model predictions [Eq. (2)] returns the thermal conductivity of the material under study.

Finally, it is important to note that the 2ω approach does not require the voltage compensation needed in the 3ω method. In the 2ω method, the extraction of the oscillating voltage from the DC signal is achieved by filtering the steady signal at the lock-in amplifier's input channel. This allows the full alternating signal sensed by the thermometer to be used for analyzing the material's thermal response. In contrast, the 3ω method requires compensating for a large $V_{1\omega}$ representing the main signal, potentially resulting in a reduced signal to noise ratio with respect to the 2ω approach.

The equipment used for our experiments comprises two lock-in amplifiers Ametek® Model 7230 DSP, a high-precision programmable resistor IET® PRS-200, plus two homemade voltage-controlled, current sources specifically designed to achieve a low thermal drift (<10 ppm/ $^{\circ}$ C).

All the measurements are performed under a high vacuum (below 10^{-4} mbar). For this purpose, the samples are installed within a test chamber that can be put under vacuum and placed inside a cryostat for low-temperature experiments (down to 50 K). Pictures of the vacuum chamber are provided in Fig. 8.

The chamber is equipped with a high-precision Pt-based temperature sensor as well as with a resistive heater. A PID feedback loop between the thermometer and the heater controls the temperature inside the chamber. A metal screen between the sample and chamber walls, regulated at the sample's temperature, guarantees a reduced impact of radiative exchange with the environment. Moreover, a homemade removable sample holder allows connecting and measuring up to four transducers at a time [Fig. 8(b)].

Thanks to this configuration, the pressure/temperature conditions inside the chamber are finely controlled. Moreover, any potential heat leaks due to radiation or non-uniform test chamber thermalization are reduced to a minimum.

IV. RESULTS AND DISCUSSION

A. Transducers calibration

The Pt transducers deposited on the SOI are calibrated by placing the sample inside the test chamber under vacuum. The temperature of the chamber is changed programmatically within a

06 January 2025 08:00:23

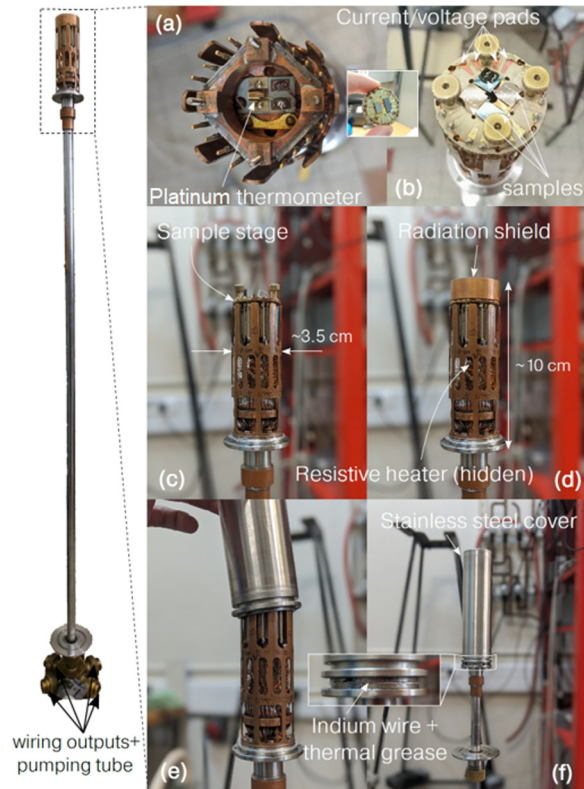


FIG. 8. Pictures of the test chamber. The chamber is shaped like a long cylindrical tube to fit inside a cryostat. Samples are attached to a circular sample holder as seen in (b) that can be removed from the chamber to allow micro-bonding. Gold pads, highlighted in red in (b), are used to electrically connect the transducers from the sample to the test chamber and acquisition system. Wires then go along the length of the tube and come out in Jaeger sockets. 4×4 pads are present to measure four samples ($I+$, $I-$, $V+$, and $V-$). The test chamber's temperature is regulated using a Pt thermometer and a resistive heater using a PID controller. (d) After screwing the copper shield to the sample holder, a stainless steel cover is screwed and sealed using an indium wire (e)–(f). The chamber is then put under vacuum using a secondary pump.

range of interest thanks to the feedback control of the heating element. After thermalization is achieved, the measured values of resistance are compared against the reference temperature given by the high-precision Pt-RTD.

Figure 9 shows the result of the calibration for the four transducers employed in the experimental campaign. TM-A and TM-B in the figure are the identical narrow transducers used in the TSD configuration, whereas TM-D and TM-C represent, correspondingly, the large and narrow transducers of the TLD configuration (see also Sec. 4 in the [supplementary material](#)). The temperature coefficient of resistance for all these 295 nm thick Pt transducers is about $2.45 \times 10^{-3} \text{ K}^{-1}$ at 300 K.

The analysis of Fig. 9 shows that the relation between the resistance and the temperature is purely linear in the temperature range tested in our study, which spans from 245 to 330 K.

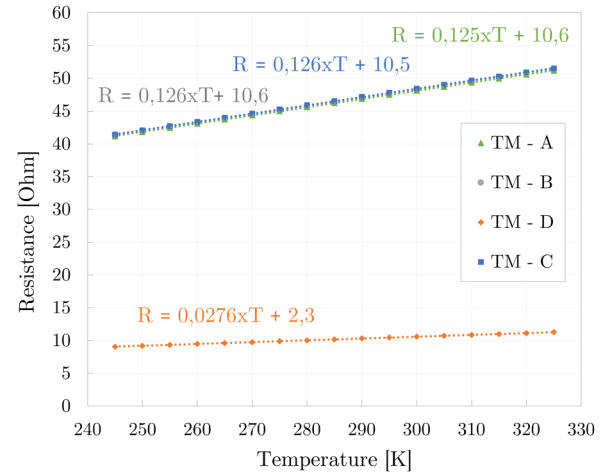


FIG. 9. Calibration curves of the four Pt/Ti transducers deposited onto the SOI sample. The transducers, TM-A, TM-B, and TM-C, are narrow transducers (around $8 \mu\text{m}$ wide), while TM-D is the large transducer ($40 \mu\text{m}$ wide).

Moreover, the three narrow thermometers exhibit a remarkably similar curve, as expected from thermometers having the same size. Knowledge of the transducers resistance and size allows determining the resistivity of the platinum lines, which in our work is around $16 \mu\text{Ohm cm}$.

B. Fitting of the 2ω experimental results

Once the thermometers are calibrated, experiments can start. Tests on the SOI are performed at four different temperatures (250, 275, 300, and 325 K) and by varying the frequency over three orders of magnitude (from 4 Hz to 4 kHz). For each tested frequency, an experimental point is obtained by averaging over 60 repeated measurements. The time between each of these measurements is scaled proportionally to the period of the AC current in order to ensure a pool of statistically independent samples, even at the lowest current frequencies. The resulting standard deviations for each experimental point are generally on the order of 10^{-7} and always below 1% of the $V2\omega$ signal (the error bars are not shown in the following pictures to improve clarity).

Moreover, for each tested temperature, data are acquired at different intensities of the AC and DC currents supplied to the heater and transducer leads. The choice of these current levels depends on balancing matters of measurement sensitivity and accuracy. Higher AC power injected into the system increases the temperature oscillation amplitude [see Eq. (2)], while higher DC power increases the 2ω voltage produced under a given temperature oscillation [see Eq. (7)]. In both cases, the signal to noise ratio is increased. On the other hand, the injected power is dissipated as Joule heating inside the test chamber, causing the local temperature of the sample to depart from the set temperature selected for the measurement. Therefore, both currents should be chosen as small as possible, so as not to reduce the accuracy of the measurements.

Finally, the DC power dissipated in the thermometer should be much lower than the AC power dissipated in the heater in order to not perturb the temperature field established by the heater. In our experiments, we tested different I_{ac} and I_{dc} levels with a maximum ratio of RI_{dc}^2/RI_{ac}^2 of around 1/6 and a minimum ratio of around 1/50. The resulting temperature trends are then normalized by the AC power supplied to the heater, which allows for comparing results at different power inputs, as shown next.

Figure 10 illustrates the 2ω results obtained with the TLD configuration at 300 K, which is predominantly sensitive to the thermal conductivity of the substrate.

Focusing first on just the experimental data, all experimental curves present very similar trends, regardless of the AC and/or DC input power. This is proof of the effective insensitivity of our tests to the AC/DC powers injected into the system.

However, the various curves overlap only up to frequencies of around 1 kHz. Discrepancies start to appear at frequencies above 1 kHz and are caused by spurious electromagnetic uptake along the measurement chain (e.g., capacitive interactions between the current leads or between the transducers and the silicon substrate). This issue sets a limit to the maximum frequency that can be measured in our experimental setup since data fitting is done by using a purely thermal model that does not account for EM effects (however, these phenomena are independent of the material thermal properties and their analysis is, therefore, not relevant to our study).

The theoretical curves in Fig. 10 are calculated using both the 3D and 2D approximation and assuming adiabatic BC. These boundary conditions are preferred with respect to the isothermal BC since thermal contact with the sampleholder occurs mostly at the borders of the sample and it is mediated by a thermal grease

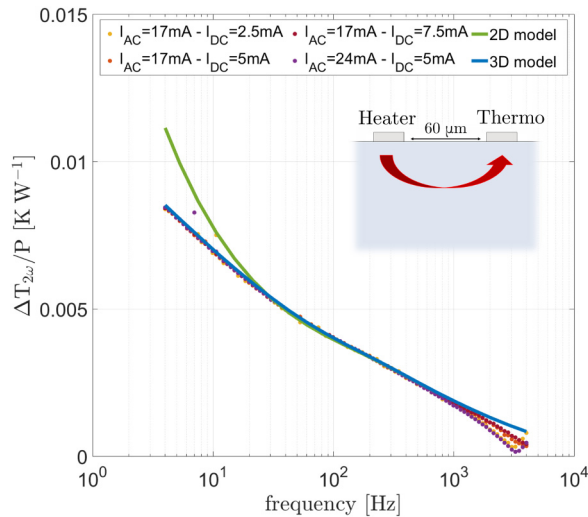


FIG. 10. Experimental and simulation results for the 2ω method with the TLD configuration at 300 K. The experimental curves are obtained at different heater (I_{AC}) and transducer (I_{DC}) currents. The model assumes adiabatic BC. The curve is fit using $k_{\text{substrate}} = 139 \text{ W m}^{-1} \text{ K}^{-1}$.

with relatively low thermal conductivity. Moreover, the experimental data are fit inserting the following substrate thermal conductivity in the model: $k_{\text{substrate}} = 139 \text{ W m}^{-1} \text{ K}^{-1}$ (other parameters being uninfluential).

Figure 10 reveals that the 2D model fits well the data only in the range between 30 and 1000 Hz, whereas the 3D approximation produces excellent agreement down to the smallest frequency. The deviation of the 2D model is attributed to the onset of 3D effects: at these low frequencies, the penetration of the heat front is comparable to the transducer's half length, resulting in a higher influence of edge effects. When frequencies increase above 30 Hz, the penetration of the heat front is reduced and the experiments become insensitive to edge effects. In this region, the heat transfer can be effectively considered as 2D and both models predict the same temperature trends.

Despite the enhanced accuracy offered by the 3D model, data fitting primarily relied on the 2D approximation, which allows for shorter computation times. However, the 3D approximation was employed "a posteriori" to verify the fitting accuracy across the entire frequency spectrum.

Figure 11 depicts the 2ω method results acquired using the TSD configuration at 300 K, intended for extracting the thermal conductivity of the thin film. The experimental curves are fitted inserting the following values in the thermal model: $k_{\text{substrate}} = 139 \text{ W m}^{-1} \text{ K}^{-1}$, $k_{\text{SiO}_2} = 1.46 \text{ W m}^{-1} \text{ K}^{-1}$, $k_{\text{film}} = 110 \text{ W m}^{-1} \text{ K}^{-1}$ (other parameters being uninfluential).

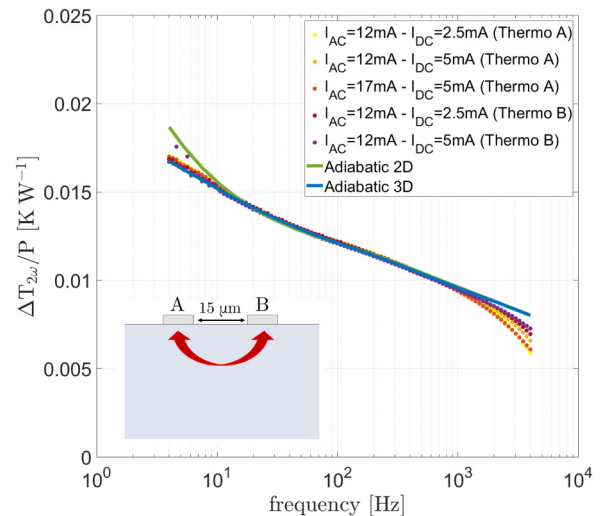


FIG. 11. Experimental and simulation results for the 2ω method of the TSD configuration (300 K). The experimental curves are obtained at different currents of the heater (I_{AC}) and transducer (I_{DC}) and switching the position of the heater and thermometer. The model assumes adiabatic BC. The experimental curves are fitted by using $k_{\text{substrate}} = 139 \text{ W m}^{-1} \text{ K}^{-1}$, $k_{\text{SiO}_2} = 1.46 \text{ W m}^{-1} \text{ K}^{-1}$, $k_{\text{film}} = 110 \text{ W m}^{-1} \text{ K}^{-1}$. The labels Thermo A and Thermo B in the legend designate experiments in which the thermometer is the sensing element A and B, respectively.

06 January 2025 08:00:23

Analogous to the TLD results, the experimental curves at different power exhibit significant overlap, particularly up to approximately 1 kHz. The overlap persists even when the roles of heating and sensing elements are interchanged—a possibility enabled by the symmetry of the TSD configuration. The labels Thermo A and Thermo B in the legend of Fig. 11 designate experiments in which the thermometer is the sensing element A and B, respectively. The consistency of these results suggests the absence of fabrication defects and electrical issues within the heater/thermometer pairs.

Regarding fitting, the divergence at lower frequencies of the 2D model is still present. However, it is less pronounced compared to the TLD case and ceases at earlier frequencies. This can be attributed to the higher aspect ratio and the reduced distance between the heating and sensing elements in the TSD configuration, suggesting that edge effects are less significant when metal lines are thinner and closer.

Finally, it should be noted that fitting of the TSD requires preliminary knowledge of both the substrate and BOX thermal conductivity. As explained in Sec. III C, determining the latter necessitates conducting additional 3ω experiments on different samples with varying SiO_2 layer thicknesses. Section 5A of the supplementary material details the data fitting for the 3ω experiments used to measure the BOX.

C. Thermal conductivity results

As mentioned in Sec. III C, the substrate's thermal conductivity can be directly derived by fitting the 2ω experiments of the TLD configuration. In contrast, extracting the BOX thermal conductivity is more involved, requiring measurements of samples at various BOX thicknesses, as detailed in Sec. 5B of the supplementary material.

Once the substrate and silica thermal conductivities are determined, the 2ω results of the TSD configuration can be fitted to extract the in-plane thermal conductivity of the Si overlayer. At this stage, all layers of the stack become known, except for the superficial TBR, the value of which is not required in our approach. However, if desired, its value can still be computed by conducting additional 3ω experiments on the full SOI stack. Section 6 in the supplementary material elucidates this procedure and presents estimates of all the thermal resistances present in the SOI sample, including those of the superficial and intermediate TBRs.

Figure 12 summarizes the thermal conductivity trends for each of the three layers composing the SOI stack. The error bars in the figure are calculated considering the multivariate nature of the fitting problem detailed in Sec. III C. Because fitting the experiments involves multiple curves with their associated uncertainties and dispersions, different combinations of the sample thermal conductivities (k_{film} , k_{BOX} , $k_{substrate}$) can achieve acceptable fits. To address this complexity, the error bars are determined through a Monte Carlo-style approach. Specifically, we generate random samples of the parameters to be fitted (i.e., the various k_{th} values of the materials), run the thermal model using these sampled values, evaluate the fit with the experimental data, and analyze the resulting variability to assess the uncertainties in the parameters.

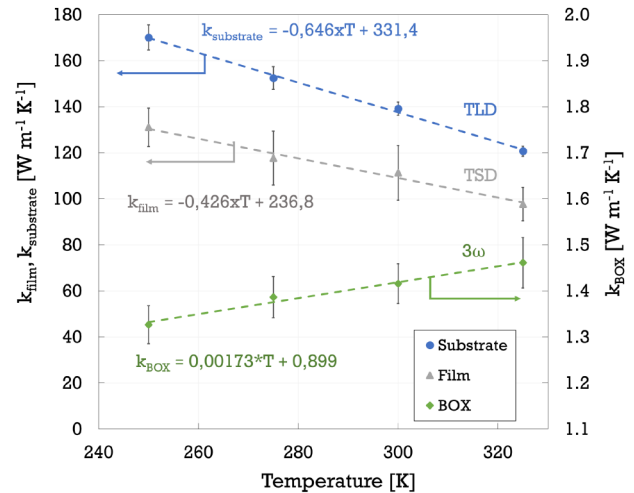


FIG. 12. Intrinsic thermal conductivities of the SOI stack layers at different temperatures, with k_{BOX} values given in the secondary axis.

In practice, for each tested temperature, a random number generator creates multiple sets of thermal conductivities (k_{film} , k_{BOX} , $k_{substrate}$) that serve as inputs for the model. Typically, the initial combinations of parameters do not fit the experimental data directly. Therefore, the thermal conductivities for each layer are iteratively adjusted, as described in Sec. III C, until a satisfactory fit is achieved. This procedure yields distributions of thermal conductivities values (k_{film} , k_{BOX} , $k_{substrate}$) that align with the experimental data. The average and twice the standard deviations of these populations are used to evaluate the mean and uncertainty of the curves shown in Fig. 12.

The curves for both Si bulk and thin film thermal conductivities in Fig. 12 are both linearly decreasing with temperature, as expected for crystalline silicon around ambient temperature. However, the thin film's curve exhibits a reduction of the in-plane conductivity of around 20% with respect to the bulk.

The thermal conductivity reduction of the monocrystalline Si thin film has been well documented in the past, and its origins are now well understood. Heat conduction in silicon is dominated by phonon transport, even in the presence of large concentrations of free charge carriers. Consequently, the decrease in thermal conductivity observed in Si thin films can be attributed to increased phonon scattering mechanisms within the layer, which typically have a limited impact in the bulk material.²² In particular, the main effect of size reduction is to greatly enhance boundary scattering at interfaces, whereas modifications to the thermal conductivity due to phonon confinement (intended here as changes to the dispersion relation due to dimensionality reduction) play a minor role in the thickness range examined here.²³ Hence, surface scattering plays the dominant role; surface oxidation and roughness at the boundary impede the propagation of phonons with long mean-free paths and consequently restrict the thermal conductivity of thin silicon films.⁹

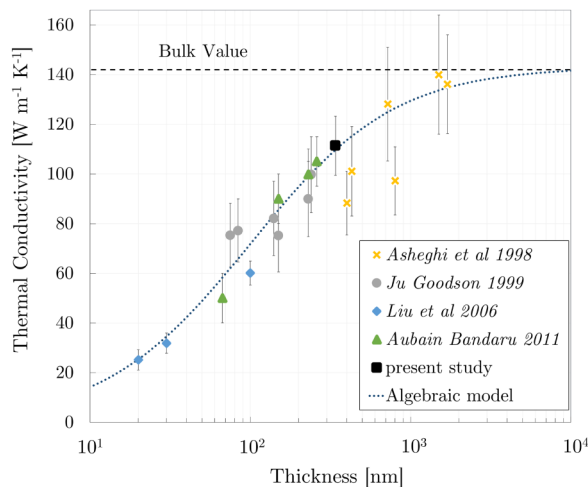


FIG. 13. Intrinsic, in-plane thermal conductivity of the monocrystalline silicon film as a function of the film thickness.

In our experiments, the reduction of the in-plane thermal conductivity with respect to bulk decreases with temperature, going from -23% at 250 K to -19% at 330 K. This trend is also understood in terms of dominant phonon wavelength decrease with increasing temperature, leading to a reduced influence of dimensional and boundary effects on the phonon transport.

Finally, Fig. 13 shows the results of different studies that measured the intrinsic, in-plane thermal conductivity reduction of the nanometric silicon film with respect to the bulk value.^{22–25} To fit the data in the graph, we implemented the algebraic model developed by Liu *et al.*,²⁴ which is an extension of the integral model of Holland.²⁶ The model is valid at room temperatures or above, and it accounts for scattering of phonons on boundaries, isotopes, and dopant elements.

Looking at Fig. 13, the result of our study aligns well with those of other works and with the results predicted by the theoretical model. Specifically, our result at 300 K indicates a thermal conductivity of the thin film equal to $k_{film, in-plane} = 111 \pm 12 \text{ W m}^{-1} \text{ K}^{-1}$, representing a 20% reduction compared to the bulk value. This good agreement is achieved by conducting tests directly on the multilayer SOI stack, thereby avoiding the need for complex nanofabrication processes to create suspended membranes and eliminating the necessity of measuring the thermal resistance of the top passivating layer.

V. CONCLUSION

A new experimental approach is presented that combines independent 2ω and 3ω measurements to accurately determine the in-plane thermal conductivity of conductive thin films. This method is particularly suitable for films grown on multilayer stacks containing insulating materials, such as SOI or GOI stacks.

The most significant feature of the proposed procedure is its insensitivity to the thermal resistance of the passivating overlayer

and, to a large extent, to any intermediate thermal boundary resistance. This characteristic allows for accurate estimation of the film's thermal conductivity by conducting experiments directly on the multilayer stack, eliminating the need for complex nanofabrication processes required to decouple the film from the substrate, such as the production of suspended samples.

The approach was validated on an SOI substrate with a 340 nm thick Si overlayer and a $1 \mu\text{m}$ thick BOX, within a temperature range of 250–325 K. The results successfully reproduced the reduction in the thermal conductivity of the Si film due to size reduction effects. Our work demonstrates the method's suitability for characterizing thermally conductive thin films and opens the way for its application in studying the thermal properties of materials such as crystalline metals and semiconductors, graphene, and other 2D and nanostructured materials.

SUPPLEMENTARY MATERIAL

See the [supplementary material](#) for details on the complete SOI stack specification (Sec. 1), the 3D thermal model of a multilayer stack (Sec. 2), the sensitivity definition used in this work (Sec. 3), the transducers design and fabrication (Sec. 4), the measurement of the BOX using the 3ω applied to multiple film thicknesses (Sec. 5), and the analysis of the thermal resistances of the full SOI stack (Sec. 6).

ACKNOWLEDGMENTS

The authors thank the technical support provided by Institut Néel, Nanofab for clean room fabrication of the probes, especially G. Julie for her support in the sample fabrication and characterization. Pole Electronique with a special thank to C. Guttin for his valuable assistance in setting up and optimizing all the electrical and electronic equipment needed for the tests. This work was supported by the Agence Nationale de la Recherche by the project FETH (Grant No. ANR-22-CE08-0023) and project Nextop (Grant No. ANR-22-CE09-0035).

AUTHOR DECLARATIONS

Conflict of Interest

The authors have no conflicts to disclose.

Author Contributions

F. Mazzelli: Conceptualization (equal); Data curation (equal); Formal analysis (equal); Investigation (lead); Methodology (equal); Validation (equal); Writing – original draft (lead). **J. Paterson:** Conceptualization (equal); Formal analysis (supporting); Investigation (supporting); Methodology (equal); Validation (equal); Writing – original draft (supporting). **F. Leroy:** Formal analysis (supporting); Funding acquisition (equal); Investigation (supporting); Methodology (equal); Project administration (supporting); Writing – original draft (supporting). **O. Bourgeois:** Conceptualization (equal); Data curation (equal); Formal analysis (equal); Funding acquisition (lead); Investigation (equal); Methodology (equal); Project administration (lead); Supervision (lead); Writing – original draft (equal).

DATA AVAILABILITY

The data that support the findings of this study are available from the corresponding author upon reasonable request.

REFERENCES

- ¹A. D. McConnell and K. E. Goodson, “Thermal conduction in silicon micro- and nanostructures,” *Annu. Rev. Heat Transfer* **14**, 129 (2005).
- ²M. Maldovan, “Micro to nano scale thermal energy conduction in semiconductor thin films,” *J. Appl. Phys.* **110**, 034308 (2011).
- ³C. Jeong, S. Datta, and M. Lundstrom, “Thermal conductivity of bulk and thin-film silicon: A Landauer approach,” *J. Appl. Phys.* **111**, 093708 (2012).
- ⁴A. T. Ramu and J. E. Bowers, “A ‘2-omega’ technique for measuring anisotropy of thermal conductivity,” *Rev. Sci. Instrum.* **83**, 124903 (2012).
- ⁵A. Sikora, H. Ftouni, J. Richard, C. Hebert, D. Eon, F. Omnes, and O. Bourgeois, “Highly sensitive thermal conductivity measurements of suspended membranes (SiN and diamond) using a 3ω -Völklein method,” *Rev. Sci. Instrum.* **83**, 054902 (2012).
- ⁶A. Sikora, H. Ftouni, J. Richard, C. Hebert, D. Eon, F. Omnes, and O. Bourgeois, “Erratum: Highly sensitive thermal conductivity measurements of suspended membranes (SiN and diamond) using a 3ω -Völklein method erratum [Rev. Sci. Instrum. 83, 054902 (2012)],” *Rev. Sci. Instrum.* **84**, 029901 (2013).
- ⁷H. Ftouni, C. Blanc, D. Tainoff, A. D. Fefferman, M. Defoort, K. J. Lulla, J. Richard, E. Collin, and O. Bourgeois, “Thermal conductivity of silicon nitride membranes is not sensitive to stress,” *Phys. Rev. B* **92**, 125439 (2015).
- ⁸E. Chávez-Angel, J. S. Reparaz, J. Gomis-Bresco, M. R. Wagner, J. Cuffe, B. Graczykowski, A. Shchepetov, H. Jiang, M. Prunnila, J. Ahopelto, F. Alzina, and C. M. Sotomayor Torres, “Reduction of the thermal conductivity in free-standing silicon nano-membranes investigated by non-invasive Raman thermometry,” *APL Mater.* **2**, 012113 (2014).
- ⁹S. Neogi, J. S. Reparaz, L. F. C. Pereira, B. Graczykowski, M. R. Wagner, M. Sledzinska, A. Shchepetov, M. Prunnila, J. Ahopelto, C. M. Sotomayor-Torres, and D. Donadio, “Tuning thermal transport in ultrathin silicon membranes by surface nanoscale engineering,” *ACS Nano* **9**, 3820 (2015).
- ¹⁰M. Handwerg, R. Mitdank, Z. Galazka, and S. Fischer, “Temperature-dependent thermal conductivity and diffusivity of a Mg-doped insulating β -Ga₂O₃ single crystal along [100], [010] and [001],” *Semicond. Sci. Technol.* **31**, 1 (2016).
- ¹¹A. T. Ramu, N. I. Halaszynski, J. D. Peters, C. D. Meinhart, and J. E. Bowers, “An electrical probe of the phonon mean-free path spectrum,” *Sci. Rep.* **6**, 33571 (2016).
- ¹²G. Yang and B.-Y. Cao, “Three-sensor 3ω - 2ω method for the simultaneous measurement of thermal conductivity and thermal boundary resistance in film-on-substrate heterostructures,” *J. Appl. Phys.* **133**, 045104 (2023).
- ¹³H. S. Carslaw and J. C. Jaeger, *Conduction of Heat in Solids*, 2nd ed. (Oxford University Press, 1959).
- ¹⁴D. Mailet, S. André, J.-C. Batsale, A. Degiovanni, and C. Moyne, *Thermal Quadrupoles: Solving the Heat Equation Through Integral Transforms* (John Wiley and Sons, 2000).
- ¹⁵T. Borca-Tasciuc, A. Kumar, and G. Chen, “Data reduction in 3ω method for thin-film thermal conductivity determination,” *Rev. Sci. Instrum.* **72**, 2139 (2001).
- ¹⁶W. Jaber and P.-O. Chapuis, “Non-idealities in the 3ω method for thermal characterization in the low- and high-frequency regimes,” *AIP Adv.* **8**, 045111 (2018).
- ¹⁷The MathWorks Inc., Matlab version: 9.13.0 (r2022b) (2022).
- ¹⁸Y. Touloukian, R. W. Powell, C. Y. Ho, and P. G. Klemens, *Thermophysical Properties of Matter—The TPRC Data Series. Volume 2. Thermal Conductivity—Nonmetallic Solids* (IFI/Plenum, 1970).
- ¹⁹Y. S. Touloukian and E. H. Buyco, *Thermophysical Properties of Matter—The TPRC Data Series. Volume 5. Specific Heat—Nonmetallic Solids* (IFI/Plenum, 1970).
- ²⁰J. Paterson, D. Singhal, D. Tainoff, J. Richard, and O. Bourgeois, “Thermal conductivity and thermal boundary resistance of amorphous Al₂O₃ thin films on germanium and sapphire,” *J. Appl. Phys.* **127**, 245105 (2020).
- ²¹J. Paterson, “Experimental investigation of heat transport in nanomaterials using electro-thermal methods,” Ph.D. thesis (Université Grenoble Alpes, 2020).
- ²²M. Ashoghi, M. N. Touzelbaev, K. E. Goodson, Y. K. Leung, and S. S. Wong, “Temperature-dependent thermal conductivity of single-crystal silicon layers in SOI substrates,” *J. Heat Transfer* **120**, 30 (1998).
- ²³Y. S. Ju and K. E. Goodson, “Phonon scattering in silicon films with thickness of order 100 nm,” *Appl. Phys. Lett.* **74**, 3005 (1999).
- ²⁴W. Liu, K. Etesam-Yazdani, R. Hussin, and M. Ashoghi, “Modeling and data for thermal conductivity of ultrathin single-crystal SOI layers at high temperature,” *IEEE Trans. Electron. Devices* **53**, 1868 (2006).
- ²⁵M. S. Aubain and P. R. Bandaru, “In-plane thermal conductivity determination through thermoreflectance analysis and measurements,” *J. Appl. Phys.* **110**, 084313 (2011).
- ²⁶M. G. Holland, “Analysis of lattice thermal conductivity,” *Phys. Rev.* **132**, 2461 (1963).